https://doi.org/10.5194/egusphere-2026-5296
Preprint. Discussion started: 16 November 2026
© Author(s) 2026. CC BY 4.0 License.

High-resolution regional climate projections and wildfire weather danger impacts in the Macaronesian archipelagos

Jordi Rull[1], Francisco J. Expósito[1], Juan P. Díaz[1], Judit Carrillo[1], Juan C. Pérez[1], and Diamantino Henriques[2]

[1]Grupo de Observación de la Tierra y la Atmósfera, Universidad de La Laguna, Canary Islands, Spain.
[2]Departamento de Meteorologia e Geofísica, Instituto Português do Mar e da Atmosfera, Azores, Portugal.

Correspondence: Jordi Rull (alu0101616742@ull.edu.es)

Abstract. Anthropogenic climate change is progressively altering fire regimes across the North Atlantic Macaronesian archipelagos. This study projects 21st-century wildfire weather using a high-resolution (3 km) Pseudo-Global Warming (PGW) approach, integrating a Coupled Model Intercomparison Project Phase 6 (CMIP6) multi-model ensemble under two Shared Socioeconomic Pathway (SSP) scenarios: SSP1-2.6 and SSP5-8.5. Daily meteorological outputs were used to compute the empirically validated Forest Fire Weather Index (FWI). Under the end-of-century (2070–2099) SSP5-8.5 pathway, projections reveal a spatial and temporal expansion of fire danger, driven by overall warming and diminished winter precipitation. In the Canary Islands and Madeira, the Length of Fire Season (LOFS) expands by 40 to 42 days on average, with localized hotspots approaching 90 days. This asymmetric early onset eliminates the winter recovery window required for fuel moisture recharge. Conversely, the Azores maintain a resilient, humid baseline, while in Cabo Verde, decreased monsoon precipitation paradoxically restricts combustible biomass. Ultimately, the projected disappearance of the operational off-season in the most vulnerable islands necessitates a fundamental realignment of civil protection strategies toward landscape-scale prevention.

1 Introduction

The worldwide escalation of wildfire risk, driven by anthropogenic greenhouse gas emissions and the resulting 1.1 °C increase in global mean surface temperature relative to 1850–1900, represents one of the most critical challenges identified in the Intergovernmental Panel on Climate Change (IPCC) Sixth Assessment Report (IPCC, 2021, 2023). This warming trend has fundamentally altered fire regimes by intensifying vapor pressure deficit and prolonging fire-weather seasons across diverse biomes (Jolly et al., 2015; Abatzoglou et al., 2019). Recent evidence confirms that climate change increases the frequency and severity of fire weather—defined by the critical intersection of high temperatures, low relative humidity, sustained winds, and precipitation deficits—which increasingly exceeds the thresholds for effective fire suppression (Smith et al., 2020; IPCC, 2021). Furthermore, future projections across Mediterranean Europe and other high-risk regions suggest that anthropogenic warming will continue to exacerbate fire intensification throughout the 21st century (Turco et al., 2018; Di Virgilio et al., 2019).

The interval between 2023 and 2025 has seen a transition toward landscape-scale disasters that frequently overwhelm national mitigation capacities. Canada's record-breaking 2023 season consumed approximately 16.5×10^6 ha, releasing nearly

https://doi.org/10.5194/egusphere-2026-5296
Preprint. Discussion started: 16 November 2026
© Author(s) 2026. CC BY 4.0 License.

480 Mt of carbon—roughly 23 % of total global wildfire emissions for that year (Canadian Interagency Forest Fire Centre, 2024; Copernicus Atmosphere Monitoring Service, 2025). During that same season across the Mediterranean, the Alexandroupolis fire in Greece burned 90 000 ha, remaining the largest single fire event in European history and emphasizing the vulnerability of the region to hydro-climate whiplash events (EU Civil Protection Knowledge Network, 2025). This trend of exceptional activity culminated in the 2025 Iberian crisis, where a record 4.6 °C temperature anomaly facilitated fires that burned over 1 % of the total surface area of the Iberian Peninsula in just two weeks (Rodríguez Camino et al., 2025; AEMET, 2025).

Wildfire danger is systematically assessed using the Canadian Forest Fire Weather Index (FWI) system, a standard numerical rating of fire intensity based on meteorological observations (Van Wagner, 1987). The FWI has been widely adopted by the European Forest Fire Information System (EFFIS) due to its sensitivity to the four primary meteorological drivers: temperature, relative humidity, wind speed, and 24 h accumulated precipitation (Dowdy et al., 2010; Bedia et al., 2014). However, as highlighted by Carrillo et al. (2022), the FWI is characterized by a complex, non-linear scoring structure rather than a simple algebraic equation, making the sensitivity of its sub-components highly dependent on regional geography and land-use patterns (Martínez et al., 2009).

The Macaronesian archipelagos—comprising the Azores, Madeira, the Canary Islands, and Cabo Verde—occupy a unique position in the North Atlantic where large-scale atmospheric circulations intersect with complex volcanic orography. These islands host a significant density of endemic species with immense scientific and ecological value, which are increasingly vulnerable to fire-driven habitat loss (Bramwell, 1990; Irl et al., 2014). Furthermore, the region is home to a diverse and growing population that creates a highly complex wildland-urban interface. This demographic pressure is intrinsically linked to tourism—the primary economic engine. The intersection of dense urbanization and tourism-driven nature use within orographically complex forested landscapes significantly increases the vulnerability of human life and regional economies to catastrophic fire events (Carrillo et al., 2022). In such fragmented and mountainous territories, standard Coupled Model Intercomparison Project Phase 6 (CMIP6) General Circulation Models (GCMs) often lack the horizontal resolution required to resolve the steep terrain and the trade wind inversion layers that govern local fuel moisture (Carrillo et al., 2022). Previous studies have demonstrated that high-resolution regionalized projections are essential to identify shifts in severe fire weather and the projected extension of the fire season, which continental studies suggest may increase by as much as 75 days per year (Moriondo et al., 2006; Jain et al., 2017). Furthermore, while broader Mediterranean literature often utilizes thresholds as high as $\mathrm{FWI} > 60$ to denote high-impact conditions, the unique fuel connectivity and steep topography of Macaronesia dictate a lower operational threshold; consequently, an index exceeding 30 effectively defines the threshold for extreme local fire danger, generating fire behavior that frequently overwhelms direct suppression capacities (Carrillo et al., 2022).

By employing high-resolution dynamical downscaling with the Weather Research and Forecasting (WRF) model (Skamarock et al., 2008), specifically its Advanced Research core (WRF-ARW), this study establishes a comprehensive regional focus across the Macaronesian archipelagos. Future climate projections are subsequently generated utilizing the Pseudo-Global Warming (PGW) approach. Unlike traditional continuous dynamical downscaling—which forces Regional Climate Models (RCMs) directly with free-running GCMs and inevitably inherits their synoptic circulation biases—the PGW method applies

https://doi.org/10.5194/egusphere-2026-5296
Preprint. Discussion started: 16 November 2026
© Author(s) 2026. CC BY 4.0 License.

a thermodynamic climate perturbation to highly accurate historical reanalysis boundary conditions. By perturbing historical baseline data with the temperature, humidity, and geopotential height deltas derived from future Shared Socioeconomic Pathways (SSPs), the PGW framework preserves the observed sequence of historical weather events. For Macaronesia, this ensures that the complex trade wind dynamics, localized atmospheric inversion layers, and steep orographic interactions remain historically accurate, while simulating how the same physical weather patterns will behave in a warmer, more volatile future climate. Building on the regional framework established by Carrillo et al. (2022), this combined WRF-PGW approach addresses the need for localized risk assessments, providing a robust framework to guide adaptation and civil protection strategies across the Macaronesian archipelagos.

To comprehensively evaluate future projections of wildfire risk, the subsequent analysis quantifies changes in the FWI and its derived seasonal metrics—specifically those measuring cumulative severity, extreme event frequency, and fire season duration—for two future horizons: the mid-century (2030–2059) and the end-of-century (2070–2099), evaluated against a recent past baseline (1990–2019). Recognizing the inherent uncertainty in global climate mitigation efforts, the analysis contrasts two divergent SSPs: a sustainable, low-emissions scenario (SSP1-2.6) and a fossil-fuel-intensive, worst-case scenario (SSP5-8.5). Following this introduction, Sect. 2 details the geographical context of Macaronesia, the high-resolution downscaling methodology, the mathematical framework of the FWI, the observational datasets utilized, and the statistical methods applied; Sect. 3 first presents the empirical validation of the modeled fire danger against satellite observations, then evaluates projected shifts in meteorological drivers and details the statistical attribution of these drivers to future fire-weather variability, and subsequently analyzes the spatial intensification of integrated fire danger indices, shifts in intra-annual seasonality, multi-decadal climate trends, and the temporal expansion of the fire season; finally, Sect. 4 synthesizes the principal regional impacts of the projected changes, concluding with a brief outline of the operational implications for civil protection and landscape management.

2 Methods

2.1 Study area

Macaronesia is a group of four volcanic archipelagos located in the North Atlantic Ocean (Fig. 1): the Azores (Portugal), Madeira (Portugal), the Canary Islands (Spain), and the Republic of Cabo Verde (Cropper, 2013; Cropper and Hanna, 2014). Due to its wide latitudinal extension ($\approx 15\,^{\circ}\mathrm{N}$ to $40\,^{\circ}\mathrm{N}$) and the steep, rugged nature of its volcanic terrain, the region exhibits high spatial variability in its climate and associated fire danger (Cropper, 2013; Carrillo et al., 2022). The islands are characterized by their small spatial extents (ranging from tens to a few thousand km^2) and extreme vertical relief—most notably exemplified by Mount Teide on the Canarian island of Tenerife, which reaches $3718\,\mathrm{m}$ above sea level—creating an orographically complex system that requires convection-permitting simulations to accurately represent the localized atmospheric processes and wind channeling that govern regional fire weather.

The region's climate is primarily regulated by the Azores High, a semi-permanent high-pressure system whose position dictates the prevalence of trade winds and the path of North Atlantic depressions (Hurrell, 1995). The volcanic, mountainous

https://doi.org/10.5194/egusphere-2026-5296
Preprint. Discussion started: 16 November 2026
© Author(s) 2026. CC BY 4.0 License.

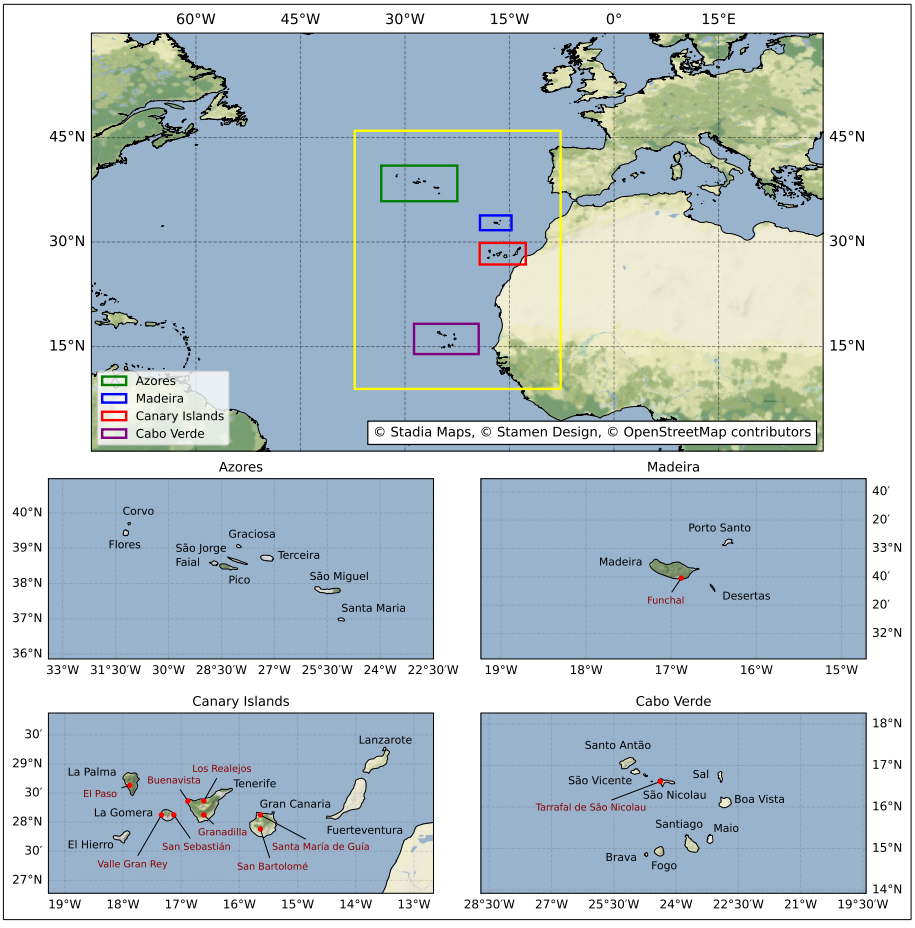


Figure 1. Geographical location and high-resolution topography of the Macaronesian archipelagos. This region is located off West Africa and Southern Europe, encompassing the archipelagos of the Azores (Portugal), Madeira (Portugal), the Canary Islands (Spain), and Cabo Verde. The main panel provides a macro-scale North Atlantic context, while the four insets correspond to the detailed convection-permitting modeling domains. These insets display high-resolution local topographic relief and major island toponymy, highlighting the 10 key hotspots with high historical burned area evaluated in the attribution analysis (these hotspot locations are indicated by red dots and distinguished with dark red labels). Map created by the authors using Python 3.12.12 with the Matplotlib 3.10.8, Cartopy 0.25.0, and Shapely 2.1.2 libraries. Topographic terrain imagery was downloaded on demand via the Stadia Maps API. Map tiles were rendered by Stadia Maps and Stamen Design (licensed under CC BY 4.0), based on OpenMapTiles (licensed under CC BY 4.0) and spatial data from OpenStreetMap contributors (released under the Open Database License, ODbL). Coastline vector data were sourced from Natural Earth, which is in the public domain (Natural Earth Terms of Use).

https://doi.org/10.5194/egusphere-2026-5296
Preprint. Discussion started: 16 November 2026
© Author(s) 2026. CC BY 4.0 License.

terrain of the islands creates distinct microclimates through orographic lift, giving rise to persistent cloud formation locally known as *sea of clouds* phenomenon (Antequera and González, 2025). For the Azores, this high-pressure system is centered to the southwest, bringing predominant westerly winds moderated by the Gulf Stream (Santos et al., 2004). In contrast, northeast trade winds are a dominant feature in the Canary Islands, creating moisture-laden windward sides and severe, fire-prone rain shadows on leeward slopes (AEMET Spain, 2012). These climatic mechanics result in four distinct fire regimes across the archipelagos. The Azores experience a humid subtropical climate with year-round precipitation that historically maintains fuel moisture above critical ignition thresholds, establishing a fire-resilient baseline (IPMA, 2025b). Madeira features a more pronounced summer dry season on its southern slopes, where dense, continuous fuel beds become vulnerable to hot easterly wind intrusions (IPMA, 2025a). The Canary Islands possess a subtropical to arid climate where the endemic *Pinus canariensis* forests are subject to extreme fire behavior during *calima* events—intrusions of hot, dry Saharan air that rapidly desiccate fuels (Carrillo et al., 2022). Finally, Cabo Verde represents a fuel-limited fire regime where the West African Monsoon dictates biomass accumulation; brief wet seasons trigger the growth of herbaceous fuels that cure during the prolonged dry season, priming the landscape for wind-driven fire spread (Neves et al., 2017; Climate Change Knowledge Portal, 2025).

2.2 Regional climate projections using the pseudo-global warming approach

High-resolution regional climate projections were generated using WRF-ARW version 3.9 within a PGW framework (Brogli et al., 2023). The selection of this specific WRF-ARW version was driven by its stability and extensive validation at the beginning of the computationally demanding, multi-year regional simulations undertaken in this study. The PGW methodology combines the realistic spatial and temporal evolution of historical weather provided by reanalysis data with the large-scale climate-change signal projected by GCMs. The approach preserves the historical sequence of synoptic weather situations while modifying their thermodynamic and dynamical characteristics according to future climate conditions. However, it is important to acknowledge the limitations of the PGW approach, particularly the fact that it does not account for future land-use changes. The progressive increase in fire activity and potential desertification can alter the surface boundary conditions of limited-area models, thereby affecting their performance and the reliability of the simulations. The regional model was configured with three one-way interactive nested domains at horizontal grid spacings of 27 km, 9 km, and 3 km, respectively. The innermost domain, covering the Macaronesian archipelagos, was run at convection-permitting resolution. The atmospheric column was discretized into 50 non-uniform vertical levels, with enhanced resolution in the lower troposphere to improve the representation of planetary boundary-layer processes and near-surface meteorological variables. The model physics configuration followed the parameterization scheme previously evaluated and applied to regional climate simulations over the study area (Expósito et al., 2015).

The recent-past reference simulation covered the 30-year period 1990–2019. Initial and lateral boundary conditions were obtained from the ERA5 reanalysis produced by the European Center for Medium-Range Weather Forecasts (ECMWF) as part of the Copernicus Climate Change Service (C3S). ERA5 provided the atmospheric and surface conditions required to initialize and force WRF throughout the baseline simulation. The resulting regional simulation constitutes the reference climate against which all future experiments were compared. Future regional projections were generated by perturbing the ERA5

https://doi.org/10.5194/egusphere-2026-5296
Preprint. Discussion started: 16 November 2026
© Author(s) 2026. CC BY 4.0 License.

initial and lateral boundary conditions according to climate-change signals derived from 17 GCMs participating in CMIP6 (Table 1) (Rodríguez-Rull et al., 2026). The climate-change signal was calculated independently for each GCM, emission scenario, future period, calendar month, atmospheric variable, and pressure level. The monthly climate-change increment was calculated as the difference between the climatological mean of the selected future period and the climatological mean of the historical period available for each individual model. The model-specific increments were subsequently averaged across the 17 GCMs to obtain a monthly multi-model ensemble-mean climate-change signal for each future period and emission scenario. The use of a multi-model mean reduces the influence of model-specific responses and provides a more robust estimate of the externally forced large-scale climate signal. The resulting three-dimensional monthly increments were interpolated horizontally and vertically to the ERA5 grid and pressure levels and temporally interpolated to the dates and times of the regional simulations. These perturbations were subsequently added to the ERA5 fields used to initialize and force WRF.

Table 1. Overview of the Coupled Model Intercomparison Project Phase 6 (CMIP6) ensemble of General Circulation Models (GCMs) used as initial and boundary conditions for the downscaling process.

GCM	Institution(s) (country)	Horizontal resolution	Reference
ACCESS-ESM1-5	CSIRO and BOM (Australia)	$1.875° \times 1.25°$	Mackallah et al. (2019)
AWI-CM-1-1-MR	AWI (Germany)	$\approx 0.9° \times 0.9°$	Semmler et al. (2020)
BCC-ESM2-MR	BCC (China)	$1.1° \times 1.1°$	Wu et al. (2019)
CanESM5	CCCma (Canada)	$\approx 2.8° \times 2.8°$	Swart et al. (2019)
CESM2	NCAR (USA)	$1.25° \times 0.9°$	Danabasoglu et al. (2020)
CMCC-ESM2	CMCC (Italy)	$2.5° \times 1.25°$	Lovato et al. (2021)
EC-Earth3	EC-Earth Consortium (Europe)	$\approx 0.7° \times 0.7°$	Döscher et al. (2022)
FGOALS-g3	CAS (China)	$2° \times 2.3°$	Li et al. (2019)
GFDL-ESM4	GFDL (USA)	$\approx 1° \times 1°$	Krasting et al. (2020)
GISS-E2-1-GN	GISS (USA)	$2.5° \times 2°$	Kelley et al. (2020)
INM-CM5-0	INM (Russia)	$2° \times 1.5°$	Volodin et al. (2018)
IPSL-CM6A-LR	IPSL (France)	$2.5° \times 1.25°$	Boucher et al. (2020)
MIROC6	JAMSTEC, AORI, NIES, R-CCS (Japan)	$1.4° \times 1.4°$	Tatebe et al. (2019)
MPI-ESM1-2-HR	MPI-M (Germany)	$\approx 0.9° \times 0.9°$	Jungclaus et al. (2021)
MRI-ESM2-0	MRI (Japan)	$1.1° \times 1.1°$	Yukimoto et al. (2020)
NorESM2-MM	NCC (Norway)	$1.25° \times 0.9°$	Selend et al. (2019)
TaiESM1	AS-RCEC (Taiwan)	$1.25° \times 0.9°$	Lee et al. (2020)

The future experiments were conducted for two 30-year periods: 2030–2059, representing mid-century conditions, and 2070–2099, representing end-of-century conditions. For each temporal horizon, two contrasting SSPs were considered: SSP1-2.6 and SSP5-8.5. SSP1-2.6 represents a low-emission pathway characterized by strong mitigation and a radiative forcing level

https://doi.org/10.5194/egusphere-2026-5296
Preprint. Discussion started: 16 November 2026
© Author(s) 2026. CC BY 4.0 License.

of 2.6 $\mathrm{W\,m^{-2}}$ by 2100, whereas SSP5-8.5 represents a high-emission, fossil-fuel-intensive pathway reaching 8.5 $\mathrm{W\,m^{-2}}$ by the end of the century.

2.3 Mathematical framework of the fire weather indices and derived metrics

To quantify long-term shifts in wildfire danger, the daily meteorological outputs from the WRF-PGW simulations were integrated into the FWI system (Van Wagner, 1987). The core calculation engine processes four primary daily meteorological variables—2 m air temperature ($^{\circ}\mathrm{C}$), 2 m relative humidity ($\%$), and 10 m wind speed ($\mathrm{km\,h^{-1}}$, derived from the 10 m zonal (east-west) and meridional (north-south) wind components) obtained at midday (12:00 UTC), alongside 24 h accumulated precipitation (mm)—over a continuous 365-day calendar sequence. The FWI is derived through a sequential, three-tiered mathematical structure. First, the daily weather inputs update three moisture codes: the Fine Fuel Moisture Code (FFMC), the Duff Moisture Code (DMC), and the Drought Code (DC), which track the progressive desiccation of superficial litter, loosely compacted organic layers, and deep organic soils, respectively. To initialize the recursive 30-year integrations, start values reflecting average spring conditions were established at 85.0 for the FFMC, 6.0 for the DMC, and 15.0 for the DC. Second, these moisture codes are combined with wind speed to compute two intermediate behavioral indices: the Initial Spread Index (ISI), representing fire propagation rate, and the Build Up Index (BUI), representing total available combustible fuel. Finally, the FWI is calculated as the non-linear combination of the ISI and BUI, providing a numerical rating of the potential frontal fire intensity.

Because the FWI is an exponential representation of fire danger, extreme values disproportionately affect the physical difficulty of fire suppression. To account for this non-linearity when evaluating seasonal averages, the FWI was transformed into the Daily Severity Rating (DSR) using the standard power-law relationship, $\mathrm{DSR} = 0.0272 \times \mathrm{FWI}^{1.77}$ (Van Wagner, 1987). By computing the annual spatial and temporal mean of the DSR, the Seasonal Severity Rating (SSR) was derived to provide a robust climatological indicator of cumulative seasonal fire stress. Furthermore, the daily time series were processed to extract the annual 90th percentile of the FWI (FWI90), a metric specifically utilized to isolate the magnitude of peak extreme danger days independent of baseline seasonal averages.

To evaluate the temporal expansion and frequency of extreme fire weather, two additional categorical indices were constructed. The Frequency of Thresholds (FOT) was calculated as the annual fraction of days where the FWI exceeds designated critical bounds, such as the FOT30 representing the percentage of days where $\mathrm{FWI} > 30$. As demonstrated by Carrillo et al. (2022), this specific threshold is highly representative of regional extreme fire danger: historical analyses of the Canary Islands indicate that over 80 $\%$ of significant fires (burning more than 30 ha) occur under conditions where the FWI exceeds this value. The operational duration of the fire season, designated as the Length of Fire Season (LOFS), was defined using a rigorous sustained-danger algorithm based on foundational Mediterranean climate studies (Moriondo et al., 2006; Bedia et al., 2014; Carrillo et al., 2022): a meteorological fire season was considered active when a grid point registered a baseline FWI value greater than or equal to 15 for a continuous streak of at least 14 consecutive days. The LOFS is subsequently extracted as the absolute temporal difference in days between the cessation and the onset of these validated danger streaks. To ensure statis-

https://doi.org/10.5194/egusphere-2026-5296
Preprint. Discussion started: 16 November 2026
© Author(s) 2026. CC BY 4.0 License.

tical integrity across the high-resolution grid, spatial terrestrial masks were strictly enforced, and domain-specific bounding thresholds were applied to dynamically filter out unphysical outliers typical of high-resolution coastal boundary modeling.

2.4 Observational datasets

To establish quantitative confidence in the WRF-PGW projections, the modeled meteorological outputs—specifically the FWI and its derived temporal boundaries—must be empirically validated against a historical climatological baseline. To achieve this, observational ground-truthing was conducted using the C3S Fire Climate Change Initiative (FireCCI) dataset. Providing a consistent, spatially explicit record of global fire occurrence, the FireCCI51 Burned Area product (Lizundia-Loiola et al., 2020) details actual burned extents and ignition timings. Crucially, the 250 m spatial resolution of this product—derived from Moderate Resolution Imaging Spectroradiometer (MODIS) surface reflectance bands—minimizes spatial uncertainty when correlating physical fires to the high-resolution modeled regional grids. While the overarching climatological baseline for the WRF historical simulations spans a 30-year period (1990–2019), the observational validation was necessarily constrained to the 2001–2019 window. This narrowing was dictated by the temporal coverage of the dataset; 2001 represents the first complete year of reliable, continuous data from the FireCCI51 series. Utilizing this 19-year satellite-era baseline, the monthly climatology of the modeled FWI was compared against the observed FireCCI51 burned-area distribution and the recorded number of fires. This temporal correlation validates whether the seasonal progression of modeled meteorological fire danger accurately reflects the historical timing of actual landscape-scale fire activity. Finally, aggregating the total monthly burned area provides the landscape-scale metric necessary to identify the non-linear tipping points where extreme FWI values overpower suppression efforts and translate into extensive spatial spread.

2.5 Statistical methods

To validate the projected anomalies in future fire danger, hypothesis tests were conducted comparing the mean FWI and its derived seasonal metrics between the historical baseline (1990–2019) and the future horizons (2030–2059, 2070–2099 under SSP1-2.6 and SSP5-8.5). Because meteorological fire danger variables often exhibit highly skewed, extreme distributions, statistical significance was determined using a rigorous, non-parametric bootstrapping technique (Efron, 1979). This approach isolates regions where the anthropogenic climate change signal clearly exceeds historical inter-annual variance without requiring assumptions about the underlying data distribution. The bootstrap procedure was executed independently at each spatial grid point using a fully vectorized 3D resampling engine. For each pixel, the 30-year chronological arrays from the recent past and future periods were resampled with replacement to generate 1000 bootstrap replicates. For each of the 1000 iterations, the difference between the resampled future and historical means was computed, constructing a robust empirical distribution of the projected climate anomaly. Exact two-tailed 95 % confidence intervals were derived directly from the 2.5th and 97.5th percentiles of this empirical distribution. The null hypothesis of no significant change was rejected (indicating a statistically significant climate change signal at the $\alpha = 0.05$ level, equivalent to $p < 0.05$) if zero fell entirely outside this confidence interval. In all spatial anomaly maps presented in this study, pixels failing this significance test (i.e., where zero falls within

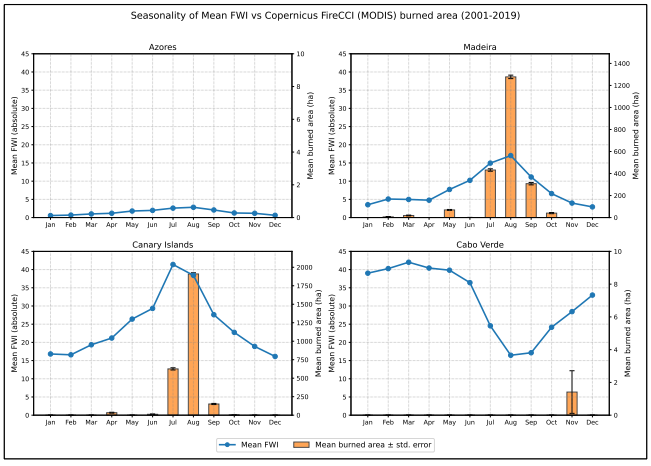
https://doi.org/10.5194/egusphere-2026-5296
Preprint. Discussion started: 16 November 2026
© Author(s) 2026. CC BY 4.0 License.

the confidence interval) are visually distinguished using dotted overlays and outlined with a thin black contour to explicitly demarcate areas of projection uncertainty.

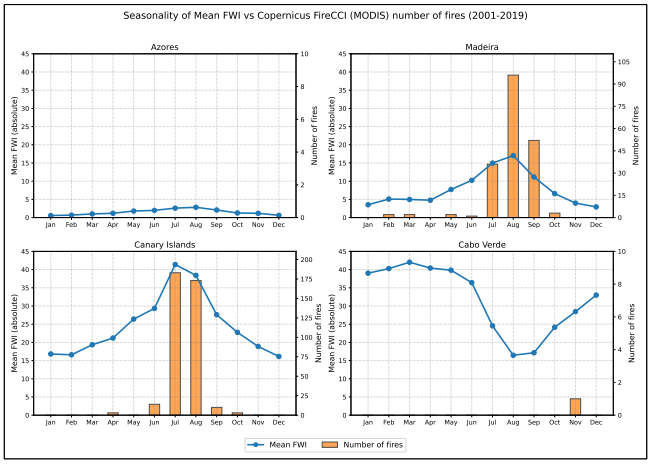
3 Results and discussion

3.1 Validation of modeled Fire Weather Index against observed fires and burned area

To assess whether seasonal fire weather severity is reflected in landscape-scale fire activity, Fig. 2 compares the monthly climatology of mean FWI with the observed FireCCI51 burned-area distribution and number of fires during 2001–2019. Because the analysis is based on monthly climatological averages rather than individual fire events, the comparison isolates the seasonal consistency between meteorological fire danger and historical landscape-scale fire activity.



(a) Mean burned area



(b) Number of fires

Figure 2. Monthly climatology of WRF-modeled mean Fire Weather Index (FWI, blue lines) compared against historical fire activity (orange bars) for the 2001–2019 period across the Macaronesian archipelagos. (a) Mean monthly burned area (ha) and (b) mean monthly number of fires, both derived from the Copernicus FireCCI dataset. Error bars denote the standard error of the mean. Values represent macro-regional monthly aggregates for each domain.

In Madeira and the Canary Islands, the seasonal progression of mean FWI corresponds with the temporal distribution of fire activity. In the Canary Islands, the FWI reaches its maximum in July, which coincides with the peak in the number of recorded fires, while the maximum burned area is reached slightly later in August. In Madeira, the FWI, the total burned area, and the number of fires all peak during August. Furthermore, Madeira exhibits a broader window of sustained fire occurrences extending into September. While burned area is influenced by fuel characteristics, anthropogenic factors, and suppression effectiveness, this seasonal agreement indicates that the WRF-modeled FWI adequately represents the underlying meteorological forcing associated with large and frequent fires in these Mediterranean-type regimes. Conversely, the Azores and Cabo Verde exhibit distinct fire behaviors. In the Azores, there is a complete absence of recorded burned area throughout the year, matching

https://doi.org/10.5194/egusphere-2026-5296
Preprint. Discussion started: 16 November 2026
© Author(s) 2026. CC BY 4.0 License.

the extremely low absolute FWI values (which peak below 4 in late summer). This reflects the persistence of humid maritime conditions and fuel characteristics that limit sustained, large-scale fire spread detectable at the 250 m satellite resolution. In Cabo Verde, the data reveal a paradoxical relationship consistent with a highly fuel-limited regime: FWI remains high from January through May, yet virtually zero fire activity is recorded. Instead, a distinct spike in both burned area and the number of fires occurs exclusively in November, as the FWI begins to rebound from its late-summer minimum following the monsoon season. This suggests that in Cabo Verde, the timing of fires is governed not by peak atmospheric aridity alone, but by the ephemeral availability of dry biomass immediately following the wet season. In essence, the Azores and Cabo Verde represent opposite fire-climate regimes: the Azores combine abundant fuel with persistently low FWI, while Cabo Verde has scarce fuel but frequently high FWI. In both cases, the net wildfire risk remains historically low. Collectively, these contrasting regional responses support the applicability of the modeled FWI in representing the diverse climatological fire regimes native to Macaronesia.

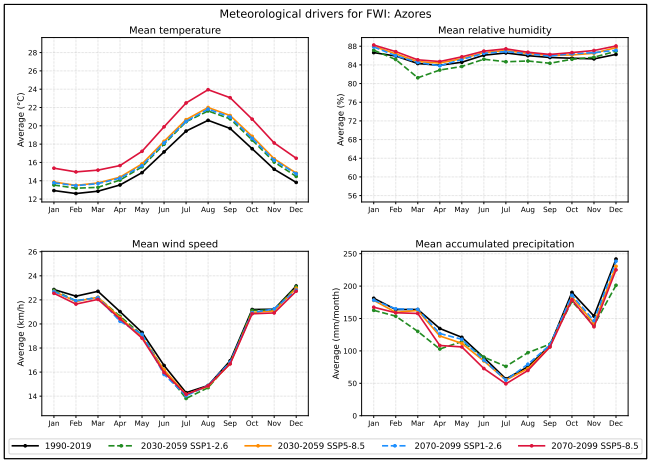
3.2 Projected shifts in meteorological drivers

Before evaluating the integrated fire danger indices, it is essential to quantify the individual perturbations of the four foundational meteorological drivers: temperature, relative humidity, wind speed, and accumulated precipitation (Fig. 3). It is important to note that to strictly adhere to the FWI mathematical framework, mean temperature, relative humidity, and wind speed are derived from midday (12:00 UTC) values rather than 24-hour daily averages. This accurately captures the peak diurnal thermo-hygrometric stress driving fire danger. Across all four archipelagos, the dominant projected climate signal is a systematic increase in mean temperature that scales directly with radiative forcing and culminates in the largest projected summer and early-autumn warming by the end of the century (2070–2099) under SSP5-8.5. Notably, mean wind speeds remain remarkably stable or exhibit only marginal declines across all domains and scenarios. This structural stability indicates that the projected intensification of future fire weather in Macaronesia will not be driven by shifting wind patterns, but predominantly by intense warming, severe atmospheric drying, and seasonal precipitation deficits.

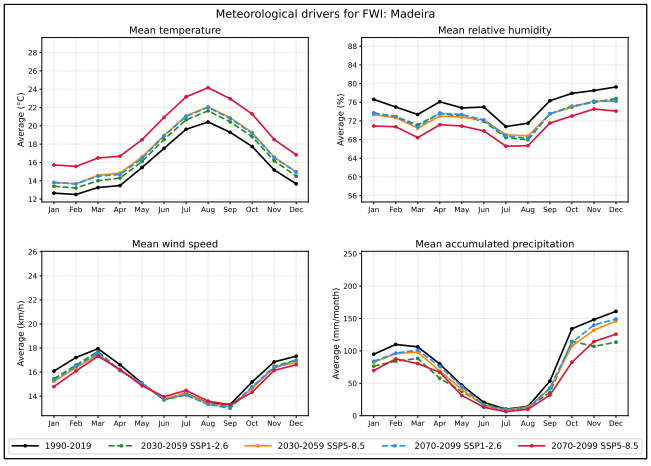
In the Canary Islands and Madeira, the projected thermal intensification is coupled with a substantial reduction in winter precipitation. The historical baseline exhibits critical winter rainfall peaks necessary for fine fuel moisture recovery. In future scenarios, this precipitation is expected to decline substantially; for instance, the Canary Islands project a near-halving of accumulated precipitation during the peak winter months under SSP5-8.5 for the 2070–2099 horizon. This severe winter drying, combined with clear decreases in summer relative humidity, prevents adequate fuel moisture recharge and establishes a highly volatile, desiccated baseline entering the peak fire season.

In contrast, the latitudinal extremes of the study area exhibit distinctly different moisture responses. In the semi-arid, fuel-limited regime of Cabo Verde, temperatures rise aggressively year-round, but late-summer monsoon precipitation (August–September) projects a severe divergence: while moderate scenarios suggest slight increases, the worst-case SSP5-8.5 scenario projects a notable end-of-century decrease, dropping peak precipitation by nearly 40 %. Paradoxically, this reduction could limit biomass accumulation, potentially constraining the development of continuous fuels. Conversely, the northernmost Azores retain their humid maritime character; while temperatures increase, relative humidity remains consistently high (exceeding

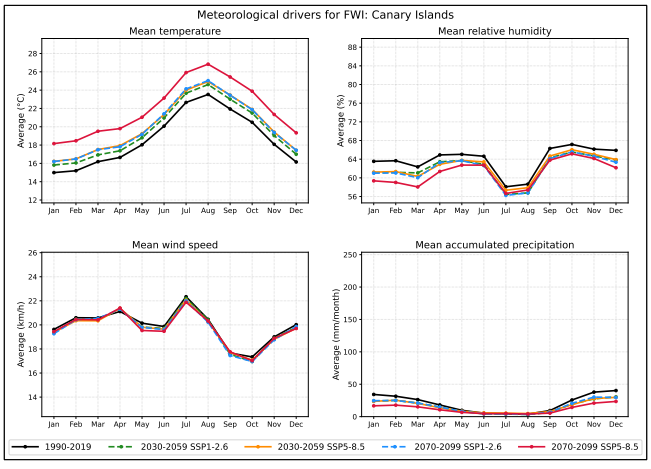
https://doi.org/10.5194/egusphere-2026-5296
Preprint. Discussion started: 16 November 2026
© Author(s) 2026. CC BY 4.0 License.



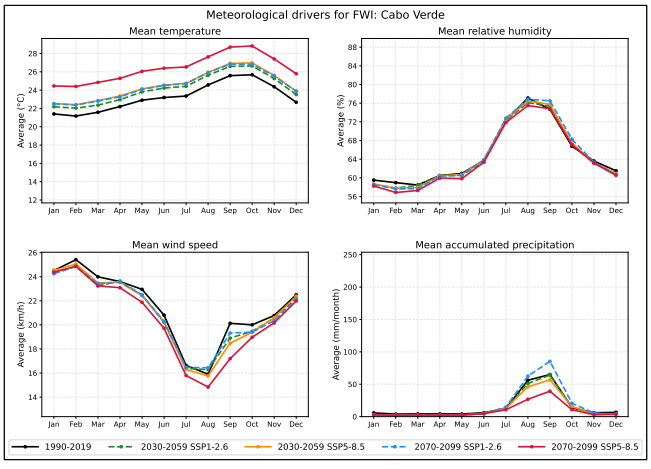
(a) Azores



(b) Madeira



(c) Canary Islands



(d) Cabo Verde

Figure 3. Projected monthly climatology of the four primary meteorological drivers of the Fire Weather Index (FWI). The panels display midday (12:00 UTC) mean temperature (°C), mean relative humidity (%), and mean wind speed ($\mathrm{km\,h^{-1}}$), plotted alongside mean accumulated precipitation ($\mathrm{mm\,month^{-1}}$). Solid black lines denote the historical baseline (1990–2019), while colored lines represent mid-century (2030–2059) and end-of-century (2070–2099) projections under the SSP1-2.6 and SSP5-8.5 pathways.

https://doi.org/10.5194/egusphere-2026-5296
Preprint. Discussion started: 16 November 2026
© Author(s) 2026. CC BY 4.0 License.

81 % year-round across all scenarios). Despite minor projected reductions in seasonal rainfall, this sustained atmospheric moisture suggests the region will remain climatologically less favorable to the widespread, meteorologically driven fire seasons projected for the lower latitudes.

3.3 Attribution and statistical drivers of Fire Weather Index

To understand the specific mechanisms forcing the projected increases in fire danger, a sensitivity analysis was conducted to isolate the individual contributions of meteorological drivers to the total change in FWI (2070–2099 SSP5-8.5 vs. 1990–2019 baseline). As illustrated in Fig. 4, the dominant factors escalating future fire danger across 10 hotspots with high historical burned area are reductions in precipitation and relative humidity. In the Canary Islands and Madeira, this atmospheric drying and lack of rainfall account for the largest share of the FWI increase, particularly during the winter and spring months. Temperature exerts a consistent, year-round upward pressure on FWI across all domains; however, its absolute monthly contribution is frequently surpassed by the moisture deficits. Notably, in several locations (e.g., El Paso and Tarrafal), projected minor reductions in summer wind speeds act as a mitigating factor, visibly suppressing the overall seasonal FWI increase. The bootstrapped uncertainty bands ($\pm 1\sigma$) remain narrow throughout the projections, indicating high statistical confidence in the direction and magnitude of these physical attributions.

To further evaluate the independent statistical influence of these drivers, Fig. 5 presents the Spearman partial correlations alongside their 95 % confidence intervals. This approach controls for the covariance between meteorological variables, revealing their isolated effect on FWI variance. The data demonstrate that the sign of the relationships between FWI and its four meteorological drivers remains remarkably stable between the historical and future periods. However, their relative strength changes across several hotspots. While near-surface temperature maintains a clear positive correlation with FWI, this relationship tends to weaken slightly in the future scenarios. In contrast, the association of FWI with relative humidity and wind tends to strengthen in a number of locations. The magnitude and tight confidence intervals of relative humidity indicate that extreme fire danger days are overwhelmingly governed by acute atmospheric desiccation. Cabo Verde serves as an extreme example of this dynamic; notably, even under the worst-case SSP5-8.5 scenario, temperature and precipitation exert almost no independent statistical influence on its FWI variance. Ultimately, these dynamics suggest a shift towards a greater relative influence of atmospheric dryness and wind conditions on future fire-weather variability, superimposed on the overall warming-driven increase in the absolute FWI severity.

3.4 Future projections of integrated fire danger indices

Building upon the analysis of individual meteorological drivers, Fig. 6 illustrates the projected spatial intensification of integrated fire danger indices across the Macaronesian archipelagos by the end of the century (2070–2099) under the severe SSP5-8.5 pathway. The maps highlight statistically significant anomalies for the mean FWI (Fig. 6a), the FWI90 (Fig. 6b), the SSR (Fig. 6c), and the FOT30 (Fig. 6d). Widespread and significant increases across all indices indicate a future climate that is increasingly conducive to severe wildfire conditions.

https://doi.org/10.5194/egusphere-2026-5296
Preprint. Discussion started: 16 November 2026
© Author(s) 2026. CC BY 4.0 License.



Figure 4. Attribution of Fire Weather Index (FWI) changes (2070–2099 SSP5-8.5 vs. 1990–2019) across 10 hotspots with high historical burned area. The bars represent the isolated physical contribution of individual meteorological drivers (temperature, relative humidity, wind, and precipitation) to the total seasonal change in FWI. The solid black line denotes the total projected ΔFWI, with the shaded area representing $\pm 1\sigma$ bootstrapped model uncertainty.

https://doi.org/10.5194/egusphere-2026-5296
Preprint. Discussion started: 16 November 2026
© Author(s) 2026. CC BY 4.0 License.

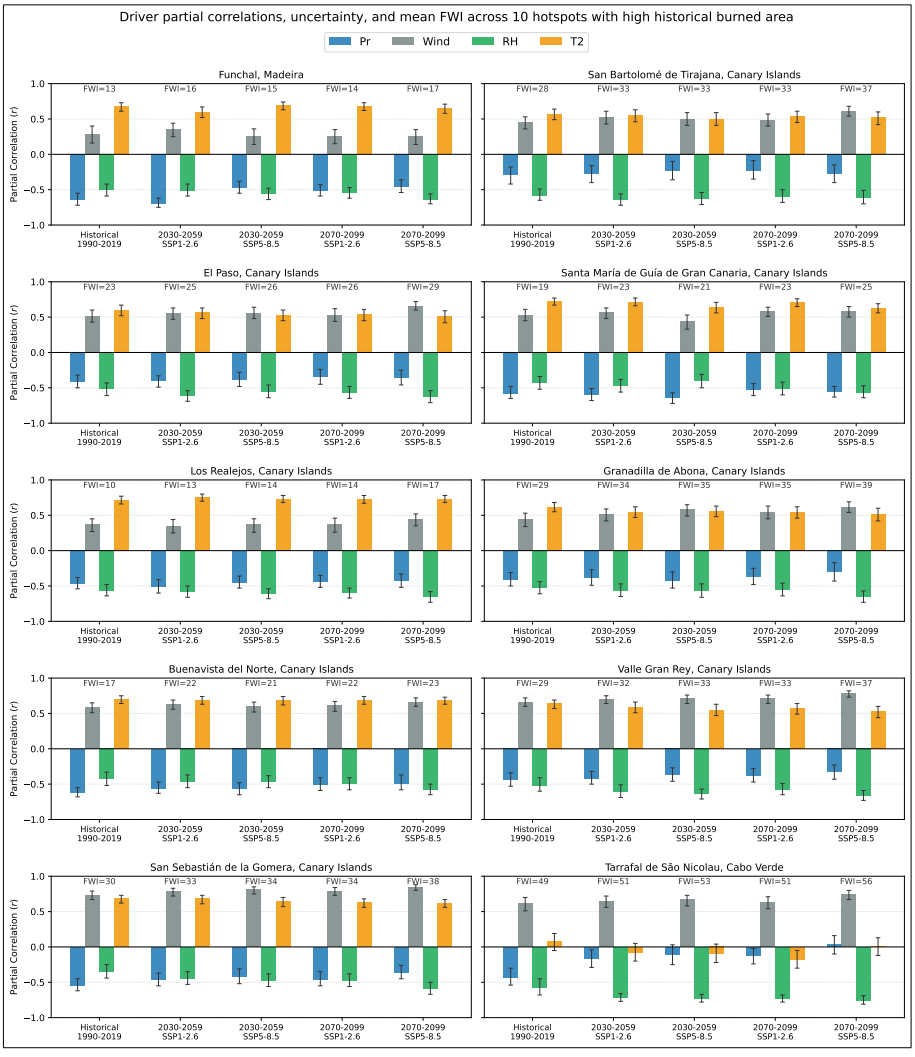
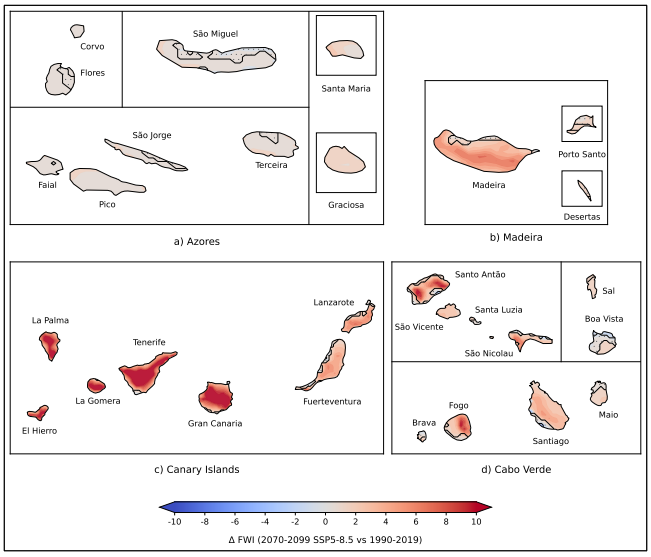
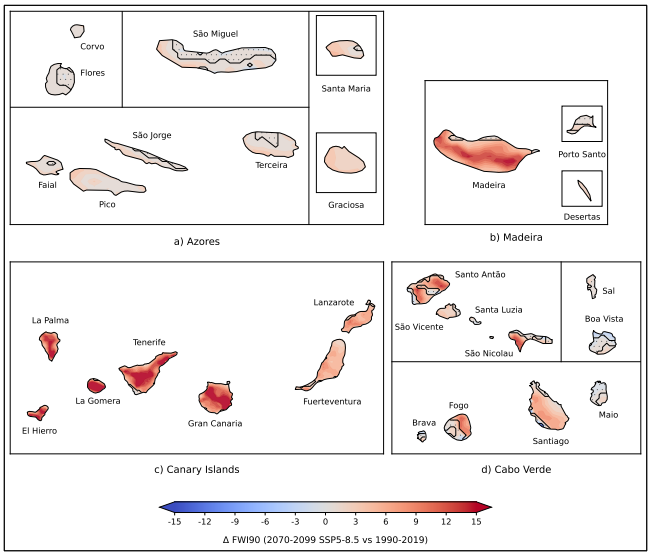


Figure 5. Spearman driver partial correlations, statistical uncertainty, and mean Fire Weather Index (FWI) across 10 hotspots with high historical burned area. The grouped bars display the isolated correlation (r) of each meteorological driver (temperature, relative humidity, wind, and precipitation) with the FWI across historical and future (SSP1-2.6, SSP5-8.5) scenarios. Error whiskers represent the 95 % confidence intervals derived via bootstrapping. The absolute mean FWI severity score for each scenario is positioned at the top of each respective set of columns.

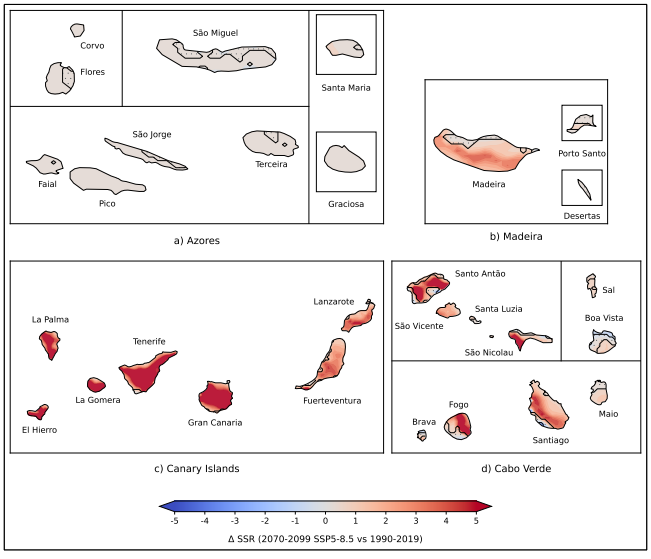
https://doi.org/10.5194/egusphere-2026-5296
Preprint. Discussion started: 16 November 2026
© Author(s) 2026. CC BY 4.0 License.



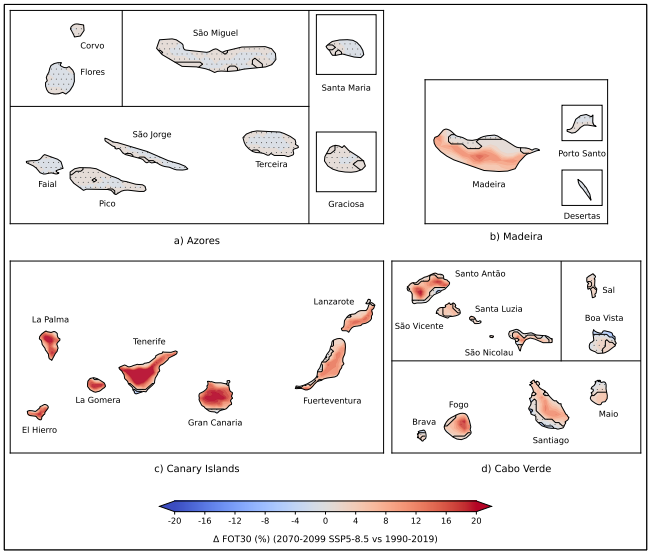
(a) Change in mean FWI



(b) Change in FWI90



(c) Change in SSR



(d) Change in FOT30

Figure 6. Spatial distribution of projected statistically significant absolute changes (Δ) in integrated fire danger indices across Macaronesia (2070–2099 SSP5-8.5 vs. 1990–2019 baseline). The panels detail shifts in (a) mean Fire Weather Index (FWI, dimensionless), (b) the 90th percentile of FWI (FWI90, dimensionless), (c) the Seasonal Severity Rating (SSR, dimensionless), and (d) the Frequency of Thresholds > 30 (FOT30, %). Positive values (warm red tones) indicate an intensification of fire danger, while negative values (cool blue tones) indicate a decrease. Hatched areas denote regions where projected changes are not statistically significant at the 95 % confidence level, as determined by the bootstrap methodology.

https://doi.org/10.5194/egusphere-2026-5296
Preprint. Discussion started: 16 November 2026
© Author(s) 2026. CC BY 4.0 License.

The most severe projected shifts occur in the Canary Islands and Madeira, regions characterized by seasonally dry subtropical fire regimes. While the mean FWI indicates widespread baseline intensification across all islands in these domains, the FWI90 reveals an even more aggressive escalation in extreme peak fire danger. This signal is spatially constrained and particularly pronounced in the topographically complex high-altitude regions. Specific focal points of extreme intensification emerge on the central peaks and eastern slopes of Madeira and Gran Canaria, the central ridge of La Palma, as well as around the Teide massif on Tenerife. The localized character of these FWI90 maxima highlights the added value of the $3\,\mathrm{km}$ convection-permitting simulations for resolving topographically complex terrain. This intensification in peak vulnerability is further exacerbated by a significant expansion in the duration of dangerous conditions, as contextualized by the SSR and FOT30 indices. By integrating the non-linear, cumulative impact of daily fire weather throughout the year, the SSR anomaly maps confirm a substantial shift toward more prolonged and punishing fire seasons overall. Crucially, the FOT30 projections demonstrate that the annual fraction of days exceeding the extreme danger threshold ($\mathrm{FWI} > 30$) will increase substantially, particularly across the Canary Islands and the southern coasts of Madeira. The combination of rising temperatures, critically reduced relative humidity, and a pronounced decline in winter precipitation across Macaronesia (Sect. 3.2) results in persistent year-round fuel drying. These projected changes are consistent with previous studies highlighting the increasing vulnerability of Mediterranean island ecosystems to prolonged drought and more frequent extreme fire weather (Carrillo et al., 2022). Specifically, this spatial pattern underscores a distinct vertical profile for extreme fire danger: the most aggressive intensification is concentrated at mid-to-high altitudes (typically above 1000–1500 m) that reside above the regional trade-wind inversion layer. In these elevated zones across Madeira and the Canary Islands, persistent atmospheric subsidence and lack of maritime moisture buffering create a critical height range where peak vulnerability is projected to escalate most severely.

In contrast, the spatial projections for the Azores show negligible statistically significant change across all four metrics. While individual meteorological variables showed minor warming trends, the derived fire danger indices remain anchored by the maritime influence of sustained high atmospheric moisture and precipitation persistence. The widespread presence of non-significant hatching across a neutral zero-anomaly baseline is consistent with the persistence of a comparatively humid climate. These results indicate that the largest projected increases in integrated fire danger are concentrated in the archipelagos of Madeira and the Canary Islands, whereas comparatively limited changes are projected for the Azores. Furthermore, most projected increases across Madeira and the Canary Islands occur within statistically significant regions, indicating that the projected climate-change signal exceeds the historical inter-annual variability estimated by the bootstrap analysis.

3.5 Intra-annual shifts and seasonality expansion

The intra-annual distribution of fire danger (Fig. 7) reveals a fundamental and systematic shift in the fire weather envelope across the latitudinal gradient. In Madeira (Fig. 7b) and the Canary Islands (Fig. 7c), the intensification is characterized by a pronounced broadening of the seasonal curve. While the summer maxima for the mean FWI and SSR increase significantly (ranging from 10 to 50 $\%$ depending on the index and region) under SSP5-8.5, the FWI90 demonstrates a parallel surge, indicating that the absolute peak severity of worst-case fire days will escalate concurrently with the seasonal average. However, the most critical shift occurs in the shoulder seasons. Specifically, the BUI demonstrates a severe lack of winter and spring recov-

https://doi.org/10.5194/egusphere-2026-5296
Preprint. Discussion started: 16 November 2026
© Author(s) 2026. CC BY 4.0 License.

ery. Historically, winter precipitation in these archipelagos allowed for significant fuel moisture recharge; however, projections indicate that heavy fuels will enter the spring at a much higher drought baseline. This creates a pre-loading effect, where the FOT30 begins to escalate as early as February in the Canary Islands and March in Madeira. In contrast, the ISI remains relatively stationary, indicating that the expansion of the fire season is driven primarily by progressive fuel desiccation rather than shifts in wind-driven propagation potential. In Cabo Verde (Fig. 7d), the seasonal cycle is governed by the West African Monsoon. While year-round thermal escalation drives the intensification of the peak FWI during the already arid spring months, the projected reduction in late-summer precipitation under SSP5-8.5 severely dampens the traditional monsoon recovery, resulting in elevated danger levels (evident in both FWI and BUI) stretching through the autumn. Conversely, the Azores (Fig. 7a) maintain their high-humidity baseline; although the mean FWI and BUI show minor upward shifts in August, the values remain well below the critical thresholds for sustained wildfire activity, confirming the archipelago's continued resilience in a warmer climate.

3.6 Multi-decadal climate trends

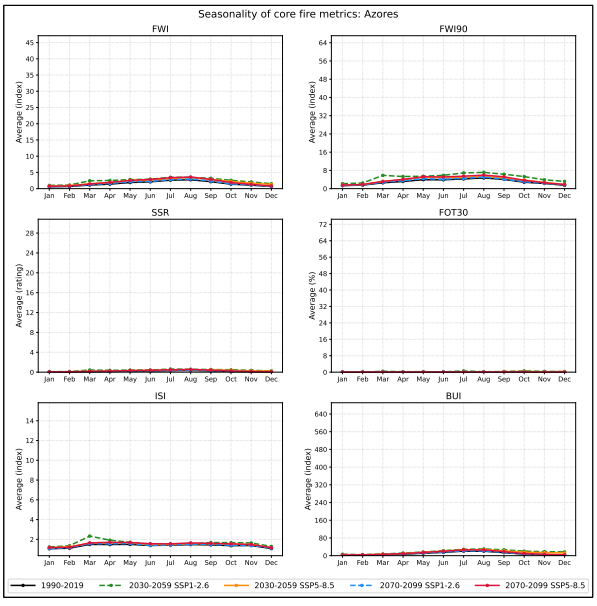
The multi-decadal evolution of fire climate indices from 1990 to 2099 (Fig. 8) illustrates a pronounced climatic shift that varies significantly by mitigation pathway. A visible divergence between scenarios emerges after 2040, an effect that is amplified across the lower latitudes but largely attenuated in the resilient maritime regime of the Azores. Under the SSP1-2.6 scenario, indices such as the FWI90 and SSR typically reach a plateau around mid-century before stabilizing, suggesting that emission mitigation limits the projected long-term increase in fire-weather danger. However, the SSP5-8.5 pathway exhibits a sustained upward trajectory across the century. In the Canary Islands (Fig. 8c) and Madeira (Fig. 8b), the LOFS displays an increasing mean alongside considerable inter-annual volatility. By the 2080s, the average LOFS under SSP5-8.5 consistently exceeds historical baseline averages; in the Canary Islands, the projected LOFS frequently surpasses even the absolute maximums recorded during the most extreme individual years of the 1990–2019 baseline, often exceeding 280 days. A notable observation is the trend in the FOT30: across the non-maritime regimes, including Cabo Verde (Fig. 8d), this metric exhibits a sustained long-term increase, indicating that extreme fire weather conditions are projected to become progressively more frequent toward the end of the century. The Azores (Fig. 8a) represent the only domain where the long-term, end-of-century trend remains relatively flat and near zero, confirming the sustained resilience of this maritime regime.

3.7 Future projections of fire seasonality

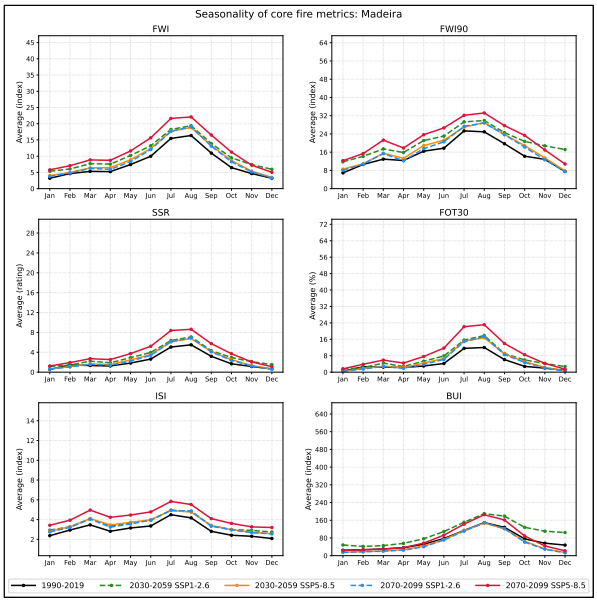
While the intensification of peak fire danger dictates the severity of individual events, the operational strain placed on civil protection agencies is largely governed by the temporal duration of the risk period. Figure 9 quantifies the projected expansion of the meteorological LOFS, pairing the spatial anomaly map (Fig. 9a) alongside the temporal shifts in season onset and cessation (Fig. 9b).

The spatial distribution reveals large and statistically significant increases in the total number of LOFS days under the end-of-century (2070–2099) SSP5-8.5 scenario. Specifically, the Canary Islands and Madeira exhibit mean temporal expansions of 40 and 42 days, respectively, across their historically fire-prone territories, with localized mid-altitude hotspots approaching

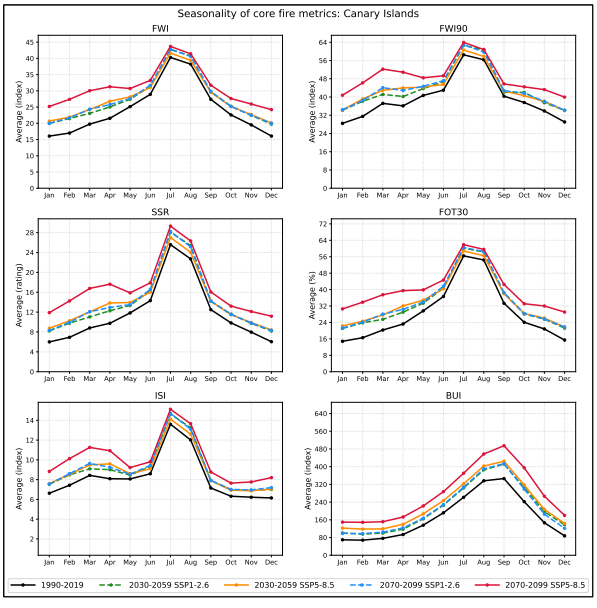
https://doi.org/10.5194/egusphere-2026-5296
Preprint. Discussion started: 16 November 2026
© Author(s) 2026. CC BY 4.0 License.



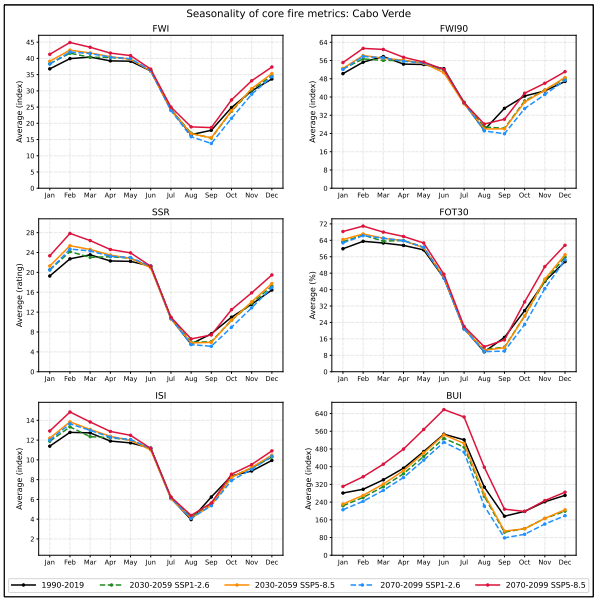
(a) Azores



(b) Madeira



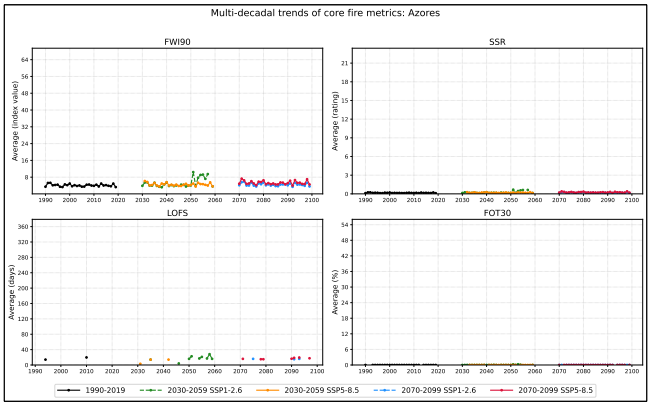
(c) Canary Islands



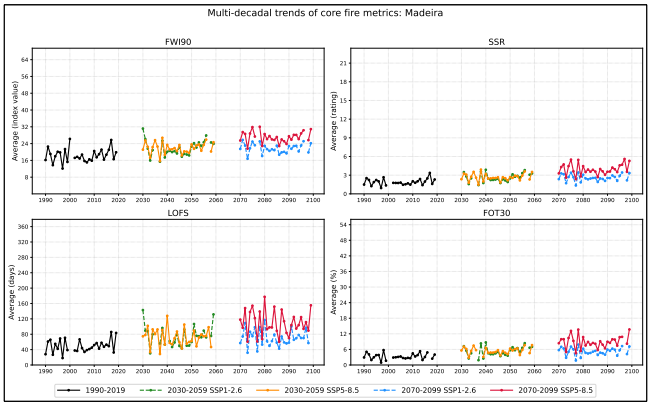
(d) Cabo Verde

Figure 7. Intra-annual seasonality of six core fire danger and behavior indices across the four archipelagos. The panels detail the monthly climatological shifts for the mean Fire Weather Index (FWI, dimensionless), the 90th percentile of FWI (FWI90, dimensionless), the Seasonal Severity Rating (SSR, dimensionless), the Frequency of Days where FWI > 30 (FOT30, %), the Initial Spread Index (ISI, dimensionless), and the Build Up Index (BUI, dimensionless). Each panel illustrates the transition from the 1990–2019 baseline (black solid line) to mid-century (2030–2059) and end-of-century (2070–2099) scenarios under the SSP1-2.6 and SSP5-8.5 pathways.

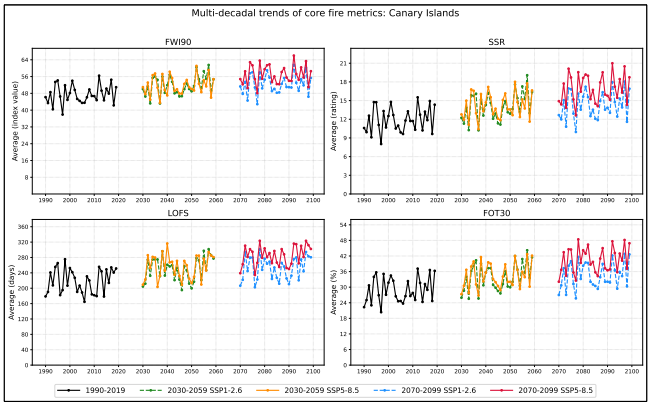
https://doi.org/10.5194/egusphere-2026-5296
Preprint. Discussion started: 16 November 2026
© Author(s) 2026. CC BY 4.0 License.



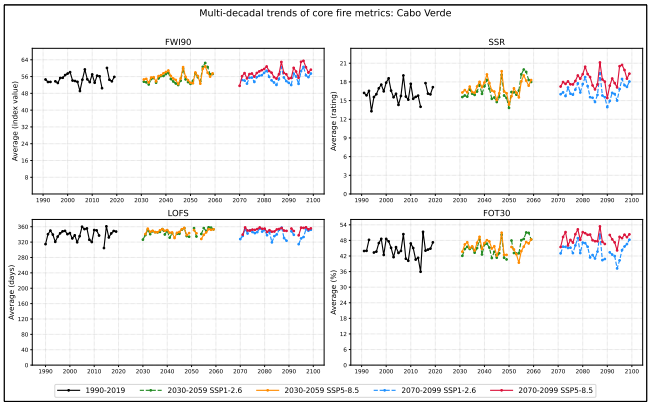
(a) Azores



(b) Madeira



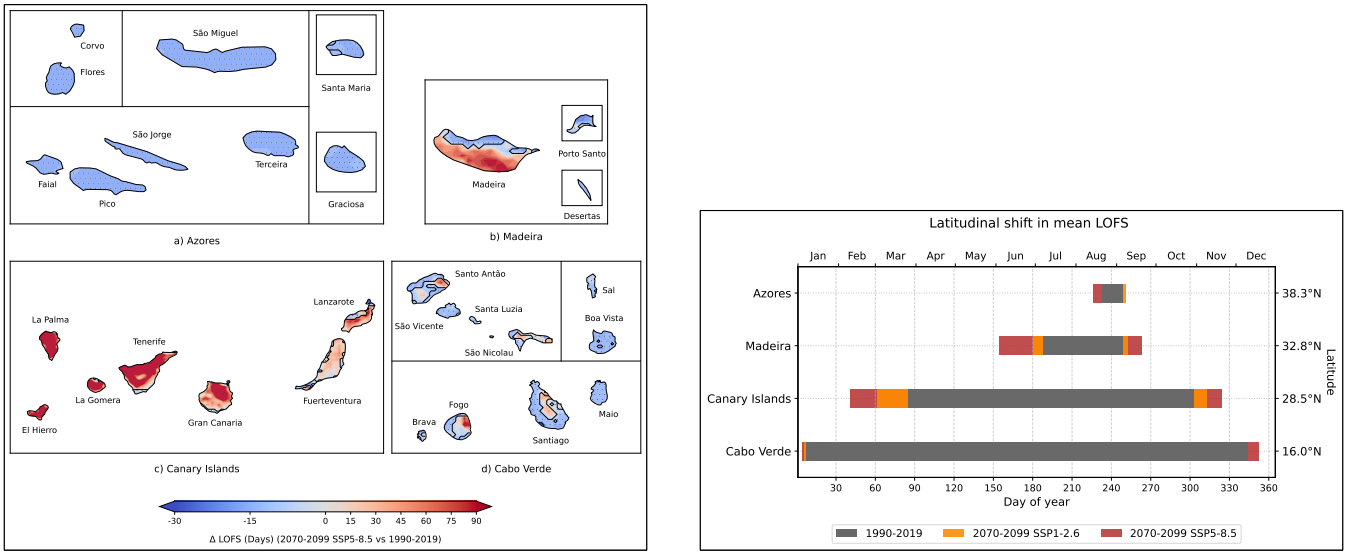
(c) Canary Islands



(d) Cabo Verde

Figure 8. Multi-decadal trends of four core integrated fire danger indices across the Macaronesian archipelagos. The data are plotted across three discrete 30-year climatological windows: historical baseline (1990–2019, black solid line), mid-century (2030–2059), and end-of-century (2070–2099). The panels track the 90th percentile of FWI (FWI90, dimensionless), Seasonal Severity Rating (SSR, dimensionless), Length of Fire Season (LOFS, days), and Frequency of Days where FWI > 30 (FOT30, %). Projections compare the high-mitigation SSP1-2.6 (dashed lines) and high-emission SSP5-8.5 (solid colored lines) scenarios.

https://doi.org/10.5194/egusphere-2026-5296
Preprint. Discussion started: 16 November 2026
© Author(s) 2026. CC BY 4.0 License.



(a) Spatial change in LOFS (days)

(b) Shift in mean LOFS timeline

Figure 9. Projected expansion of the meteorological Length of Fire Season (LOFS). Panel (a) displays the spatial distribution of statistically significant changes in LOFS duration (2070–2099 SSP5-8.5 vs. 1990–2019 baseline), with hatched areas denoting regions of statistical non-significance. Note the asymmetric colorbar scale (−30 to 90 days) required to capture the extreme non-linear expansion observed in the eastern archipelagos without visual saturation. Panel (b) illustrates the temporal expansion of the season boundaries (onset and cessation) across the latitudinal gradient, comparing the historical baseline (1990–2019, gray bars) against end-of-century (2070–2099) projections for both the SSP1-2.6 (orange bars) and SSP5-8.5 (red bars) scenarios.

a 90-day increase. This represents a structural regime shift where the meteorological fire season occupies nearly 75 % of the calendar year. Crucially, the timeline in Fig. 9b illustrates how this expansion occurs, revealing an aggressive widening of the temporal boundaries rather than just an intensification of the existing summer peak.

In the Canary Islands, the expansion is heavily asymmetric. While the cessation of the season extends deeper into mid-November, the onset of the fire season shifts approximately six weeks earlier into the spring. Under the SSP5-8.5 pathway, the historical meteorological fire season—which typically began in late March—is projected to commence by mid-February. This early onset substantially reduces the winter recovery period available for fine fuel moisture recharge and prescribed burning operations. In Madeira, the expansion follows an even more pronounced pattern; the onset pushes a full month earlier into early June, while the cessation extends significantly into late September. In Cabo Verde, while the spatial anomaly indicates a general reduction or non-significant change across much of the territory, the temporal boundaries of the season remain stretched across virtually the entire calendar year, though as previously validated, the physical realization of this danger remains dependent on anomalous wet-season fuel growth.

The projected temporal expansion across the Canary Islands and Madeira is compounded by an increase in the density of extreme days within the season. Combined with the projected increase in extreme fire-weather indices described in the previous sections, the expansion of the LOFS indicates that periods of elevated fire danger are projected to persist for substantially

https://doi.org/10.5194/egusphere-2026-5296
Preprint. Discussion started: 16 November 2026
© Author(s) 2026. CC BY 4.0 License.

longer durations. The Azores remain the contrasting response. As shown in the spatial anomaly map (Fig. 9a), although the spatial distribution exhibits slight blue-toned shifts, these changes are statistically non-significant across the entire territory, as indicated by the persistent hatching. Furthermore, the timeline (Fig. 9b) illustrates that this brief historical risk window undergoes a slight temporal contraction and a marginal shift toward late summer, rather than a structural expansion.

4 Conclusions

This study utilized a convection-permitting regional climate modeling approach (WRF-ARW) at a 3 km resolution to quantify the 21st-century trajectory of wildfire danger across the Macaronesian archipelagos. The application of the PGW methodology, coupled with CMIP6 multi-model ensemble deltas under contrasting emission scenarios (SSP1-2.6 and SSP5-8.5), isolated the impact of anthropogenic climate change while preserving the complex, localized synoptic patterns that govern the region's diverse microclimates. The projections indicate that the absolute increase in future fire weather will be primarily driven by widespread warming, reduced precipitation, and atmospheric drying. However, statistical attribution reveals a dynamical shift: future fire-weather variability will become increasingly modulated by atmospheric moisture deficits and localized wind conditions, superimposed upon this warming baseline.

The spatial and temporal escalation of projected fire danger is highly asymmetric across the latitudinal gradient. In the northernmost archipelago of the Azores, the territory remains resilient, partially buffered by its stable, humid maritime baseline. Despite projected increases in absolute near-surface temperatures, the derived fire danger indices across these islands exhibit negligible statistically significant changes. Sustained high atmospheric moisture and persistent precipitation effectively constrain the expansion of the fire season, ensuring the region remains climatologically unfavorable to the widespread, meteorologically driven fire events projected for the lower latitudes.

The Canary Islands and Madeira face the most severe disruption, exhibiting a transition toward substantially longer periods of meteorological fire danger. In these topographically complex archipelagos, the meteorological LOFS is projected to undergo mean temporal expansions of 40 and 42 days, respectively, with localized mid-altitude hotspots approaching a 90-day increase under the worst-case SSP5-8.5 pathway. Crucially, this expansion is heavily asymmetric, characterized by a pronounced advancement that shifts the start of the fire season from late March to mid-February in the Canary Islands, and from early July to early June in Madeira. This earlier onset could substantially reduce the historical winter recovery window available for fine fuel moisture recharge and proactive forest management activities, such as prescribed burning. Furthermore, a relentless, systematic increase in the frequency of extreme danger days (measured by the FOT30 metric) indicates that extreme fire weather is projected to become substantially more frequent throughout the year, compounding the difficulty of both wildfire suppression and preventive landscape management.

Conversely, the tropical southernmost archipelago of Cabo Verde presents a unique fuel-limited paradox. While projections show a significant escalation in raw fire weather indices, these will only translate to more destructive fires if there is sufficient biomass to burn. In these semi-arid environments, the projected reduction in monsoon precipitation under SSP5-8.5 may paradoxically act as a negative feedback by restricting the growth of continuous combustible biomass, even as physical temper-

https://doi.org/10.5194/egusphere-2026-5296
Preprint. Discussion started: 16 November 2026
© Author(s) 2026. CC BY 4.0 License.

atures soar. Future risk in Cabo Verde is likely to be governed by the timing of whiplash years, where anomalous wet seasons are followed by extreme spring droughts that create the necessary conditions for large-scale fire spread.

For civil protection agencies and forest managers, the projected expansion of fire-weather severity and season length highlights the increasing importance of preventive landscape management and long-term adaptation planning. As periods of elevated fire danger become more frequent and persistent, preparedness strategies must evolve alongside traditional suppression-based approaches. The combination of convection-permitting regional climate simulations, the PGW framework, and empirical validation against satellite-derived burned area observations provides confidence that the projected changes reflect physically consistent responses to anthropogenic climate change at spatial scales relevant for island fire management.

Data availability. The datasets generated and/or analyzed in this study are available from the corresponding author upon reasonable request. Following manuscript acceptance, the complete dataset will be deposited and made openly available in the Mendeley Data repository under a CC BY 4.0 license.

Author contributions. JR performed the formal analysis, developed the software, created the visualizations, and wrote the original draft. FJE, JPD, JC, and JCP supervised the research. JR, FJE, and JCP curated the data. JPD administered the project. All authors (JR, FJE, JPD, JC, JCP, and DH) contributed to the validation, as well as to the review and editing of the manuscript.

Competing interests. The authors declare that they have no conflict of interest.

Acknowledgements. This research utilized data from the World Climate Research Programme (WCRP) Coupled Model Intercomparison Project Phase 6 (CMIP6) (WCRP, 2025) and the Copernicus Climate Change Service (C3S) implemented by ECMWF. We acknowledge the valuable observational data provided by the European Space Agency (ESA) Fire Climate Change Initiative (FireCCI) for the provision of the MODIS-derived FireCCI51 global burned area dataset. The numerical modeling was performed using the WRF-ARW model (Skamarock et al., 2008), and we thank the National Center for Atmospheric Research (NCAR) and the WRF development community for making this essential open-source tool available. Data processing, analysis, and visualization were performed using the Python ecosystem, specifically the Cartopy (Elson et al., 2023), earthaccess (López et al., 2024), Matplotlib (Hunter, 2007), netCDF4 (Rew et al., 1989), NumPy (Harris et al., 2020), pandas (pandas development team, 2020), regionmask (Hauser et al., 2024), SciPy (Virtanen et al., 2020), Shapely (Gillies et al., 2025), and xarray (Hoyer and Hamman, 2017) libraries. Computational resources were provided by the Teide-HPC facility at the Instituto Tecnológico y de Energías Renovables (ITER), Canary Islands. Finally, we acknowledge the WCRP CORDEX Flagship Pilot Study on Macaronesian Archipelagos (FPS-I-Mac) for its support and focus on this region. During the preparation of this work, the authors used Google Gemini 3.1 Pro to improve readability, subsequently reviewing and editing the content as needed, and assume full responsibility for the published article.

https://doi.org/10.5194/egusphere-2026-5296
Preprint. Discussion started: 16 November 2026
© Author(s) 2026. CC BY 4.0 License.

References

Abatzoglou, J. T., Williams, A. P., and Barbero, R.: Global emergence of anthropogenic climate change in fire weather indices, Geophysical Research Letters, 46, 326–336, https://doi.org/10.1029/2018GL080959, 2019.

AEMET: Informe sobre la ola de calor de agosto de 2025 en España, Agencia Estatal de Meteorología, 2025.

AEMET Spain: Climate atlas of the Canary Islands, Madeira, and Azores archipelagos, Tech. rep., Agencia Estatal de Meteorología, https://www.aemet.es/documentos/es/conocermas/recursos_en_linea/publicaciones_y_estudios/publicaciones/2Atlas_climatologico/Atlas_Clima_Macaronesia___Baja.pdf, 2012.

Antequera, P. D. and González, J. C.: Methodological approach for the characterisation and trend analysis of subsidence thermal inversions: The case of the Canary Islands, International Journal of Climatology, https://doi.org/10.1002/joc.8933, 2025.

Bedia, J. et al.: Forest fire danger projections in the Mediterranean using ENSEMBLES regional climate change scenarios, Climatic Change, 122, 185–199, https://doi.org/10.1007/s10584-013-1005-z, 2014.

Boucher, O., Servonnat, J., Albright, A. L., Aumont, O., Balkanski, Y., Bastrikov, V., Bekki, S., Betts, R. A., Boulanger, E., Cartisano, R., Ciais, P., D'Andrea, F., Denvil, S., Devel, T., Doutriaux-Boucher, M., Dufresne, J.-L., Echevin, V., Ghattas, J., Guez, L., Hémond, P., Hourdin, F., Kageyama, M., Khodri, M., Lefebvre, M.-P., Li, L., Maignan, F., Marchand, M., Morin, E., Mignot, J., Misson, L., Möbis, B., Nabat, P., Naia, P., Peylin, P., Prévost, M., Remaud, M., Resplandy, L., Schmeits, M., Sima, A., Tachiiri, K., Terray, P., Vancoppenolle, M., Véron, L., Yelekci, M., and Zompi, F.: Presentation and evaluation of the IPSL-CM6A-LR climate model, Geoscientific Model Development, 13, 3591–3619, https://doi.org/10.5194/gmd-13-3591-2020, 2020.

Bramwell, D.: Conserving biodiversity in the Canary Islands, Annals of the Missouri Botanical Garden, pp. 28–37, https://doi.org/10.2307/2399622, 1990.

Brogli, R., Heim, C., Mensch, J., Sørland, S. L., and Schär, C.: The pseudo-global-warming (PGW) approach: methodology, software package PGW4ERA5 v1.1, validation, and sensitivity analyses, Geoscientific Model Development, 16, 907–926, https://doi.org/10.5194/gmd-16-907-2023, 2023.

Canadian Interagency Forest Fire Centre: Canada Report 2024: Annual Fire Statistics, Tech. rep., CIFFC, Winnipeg, MB, 2024.

Carrillo, J., Pérez, J. C., Expósito, F. J., Díaz, J. P., and González, A.: Projections of wildfire weather danger in the Canary Islands, Scientific Reports, 12, 8093, https://doi.org/10.1038/s41598-022-12132-5, 2022.

Climate Change Knowledge Portal: Cape Verde climatology, Tech. rep., Climate Change Knowledge Portal, https://climateknowledgeportal.worldbank.org/country/cape-verde/climate-data-historical, 2025.

Copernicus Atmosphere Monitoring Service: 2025 sees intense wildfire year in the Northern Hemisphere, Tech. rep., ECMWF, 2025.

Cropper, T.: The weather and climate of Macaronesia: past, present and future, Weather, 68, 300–307, https://doi.org/10.1002/wea.2155, 2013.

Cropper, T. E. and Hanna, E.: An analysis of the climate of Macaronesia, 1865–2012, International Journal of Climatology, 34, 604–622, https://doi.org/10.1002/joc.3710, 2014.

Danabasoglu, G., Lamarque, J.-F., Bacmeister, J., Bailey, D. A., Du's, M., Edwards, J., Fasullo, J., Garcia, R., Hannay, C., Holland, M., Johns, T. C., Lawrence, P. J., Lenaerts, J. T. M., Lindsay, K., Long, M. C., Ludescher, J., Milliman, E., Neale, R., Oleson, K. W., Otto-Bliesner, B., Polvani, L., Schmidt, G. A., Smith, R., Stösel, R. A., Tribbia, J. J., Vavrus, S., and Vertenstein, M.: The Community Earth System Model, Version 2 (CESM2), Journal of Advances in Modeling Earth Systems, 12, e2019MS001 916, https://doi.org/10.1029/2019MS001916, 2020.

https://doi.org/10.5194/egusphere-2026-5296
Preprint. Discussion started: 16 November 2026
© Author(s) 2026. CC BY 4.0 License.

Di Virgilio, G. et al.: Climate change increases the potential for extreme wildfires, Geophysical Research Letters, 46, 8517–8526, https://doi.org/10.1029/2019GL083699, 2019.

Döscher, R., Acosta, M., Alessandri, A., Anthoni, P., Arsouze, M., Bergner, J., Boussetta, S., Caron, L.-P., Cvijanovic, I., Devasthale, A., Dukhovskoy, D., Echevarria, P., Ekman, S., Evaldsson, M., Kjellström, E., Koseki, S., Lang, B., Li, C., Manrique-Suarez, M., Mantsis, D., Martin, S., Masson, S., Mensa, M., Mestre, O., Nilsson, J., Nymark, L., Parding, K. M., Perlt, H., Radu, R., Sima, A., Toniazzo, T., and Wyser, K.: The EC-Earth3 earth system model for CMIP6, Geoscientific Model Development, 15, 2633–2704, https://doi.org/10.5194/gmd-15-2633-2022, 2022.

Dowdy, A. J. et al.: Index sensitivity analysis applied to the Canadian Forest Fire Weather Index and the McArthur forest fire danger index, Meteorological Applications, 17, 298–312, https://doi.org/10.1002/met.170, 2010.

Efron, B.: Bootstrap methods: Another look at the jackknife, The Annals of Statistics, 7, 1–26, https://doi.org/10.1214/aos/1176344552, 1979.

Elson, P., de Andrade, E. S., Lucas, G., May, R., Hattersley, R., Campbell, E., Comer, R., Dawson, A., Little, B., Raynaud, S., scmc72, Snow, A. D., lgolston, Blay, B., Killick, P., lbdreyer, Peglar, P., Wilson, N., Andrew, Szymaniak, J., Berchet, A., Bosley, C., Davis, L., Filipe, Krasting, J., Bradbury, M., stephenworsley, and Kirkham, D.: SciTools/cartopy, https://doi.org/10.5281/zenodo.8216010, 2023.

EU Civil Protection Knowledge Network: Lessons learned from the 2024 fire season in Greece, Tech. rep., European Commission, 2025.

Expósito, F. J., González, A., Pérez, J. C., Díaz, J. P., and Taima, D.: High-resolution future projections of temperature and precipitation in the Canary Islands, Journal of Climate, 28, 7846–7856, https://doi.org/10.1175/JCLI-D-15-0030.1, 2015.

Gillies, S., van der Wel, C., Van den Bossche, J., Taves, M. W., Arnott, J., Ward, B. C., et al.: Shapely (2.1.2), https://doi.org/10.5281/zenodo.17193310, 2025.

Harris, C. R., Millman, K. J., van der Walt, S. J., Gommers, R., Virtanen, P., Cournapeau, D., Wieser, E., Taylor, J., Berg, S., Smith, N. J., Kern, R., Picus, M., Hoyer, S., van Kerkwijk, M. H., Brett, M., Haldane, A., del Río, J. F., Wiebe, M., Peterson, P., Gérard-Marchant, P., Sheppard, K., Reddy, T., Weckesser, W., Abbasi, H., Gohlke, C., and Oliphant, T. E.: Array programming with NumPy, https://doi.org/10.1038/s41586-020-2649-2, 2020.

Hauser, M., Spring, A., Busecke, J., van Driel, M., Lorenz, R., and readthedocs-assistant: regionmask/regionmask: version 0.12.1 (v0.12.1), https://doi.org/10.5281/zenodo.10849860, 2024.

Hoyer, S. and Hamman, J.: xarray: N-D labeled Arrays and Datasets in Python, https://doi.org/10.5334/jors.148, 2017.

Hunter, J. D.: Matplotlib: A 2D graphics environment, https://doi.org/10.1109/MCSE.2007.55, 2007.

Hurrell, J. W.: Decadal trends in the North Atlantic Oscillation: Regional temperatures and precipitation, Science, 269, 676–679, https://doi.org/10.1126/science.269.5224.676, 1995.

IPCC: Climate Change 2021: The Physical Science Basis. Contribution of Working Group I to the Sixth Assessment Report of the Intergovernmental Panel on Climate Change, Tech. rep., Cambridge University Press, https://doi.org/10.1017/9781009157896, 2021.

IPCC: Climate Change 2023: Synthesis Report. Contribution of Working Groups I, II and III to the Sixth Assessment Report of the Intergovernmental Panel on Climate Change, Tech. rep., IPCC, https://doi.org/10.59327/IPCC/AR6-9789291691647, 2023.

IPMA: Resumo climatológico: Arquipélagos da Madeira e dos Açores (2010-2025), Tech. rep., Instituto Português do Mar e da Atmosfera, ISSN 2184-9757, https://www.ipma.pt/pt/oclima/boletins/2184-9757, 2025a.

IPMA: IPMA, Tech. rep., Instituto Português do Mar e da Atmosfera, https://www.ipma.pt/en/index.html, 2025b.

Irl, S. D. H. et al.: Burned and devoured—introduced herbivores, fire, and the endemic flora of the high-elevation ecosystem on La Palma, Canary Islands, Arctic, Antarctic, and Alpine Research, 46, 859–869, https://doi.org/10.1657/1938-4246-46.4.859, 2014.

https://doi.org/10.5194/egusphere-2026-5296
Preprint. Discussion started: 16 November 2026
© Author(s) 2026. CC BY 4.0 License.

Jain, P., Wang, X., and Flannigan, M. D.: Trend analysis of fire season length and extreme fire weather in North America between 1979 and 2015, International Journal of Wildland Fire, 26, 1009–1020, https://doi.org/10.1071/WF17008, 2017.

Jolly, W. M. et al.: Climate-induced variations in global wildfire danger from 1979 to 2013, Nature Communications, 6, 7537, https://doi.org/10.1038/ncomms8537, 2015.

Jungclaus, J. H., Bittner, M., Frauen, C., Gier, B. K., Goessling, H. F., Hedemann, C., Hohl, H., Hörst, N., Löw, T., Manzini, E., Notz, D., Pless, L., Röttger, B., Schemann, V., Scholz, A., Schüpbach, E., Siegel, A., Stephan, C. C., Tews, S., Trautvetter, H., Vahl, S., Vamborg, F. S. E., Wang, Z., and Ziemen, F. A.: The MPI-ESM1.2 Earth System Model, Geoscientific Model Development, 14, 4115–4141, https://doi.org/10.5194/gmd-14-4115-2021, 2021.

Kelley, M., Schmidt, G. A., Nazarenko, L., Ruedy, R., Lea, S. A., Romanou, A., Bauer, S. E., Cox, S., DeAngelis, A., Gordon, N., Love, K. L., Mix, K., O'Meara, J., Tausnev, L., Van Lier-Walqui, H., and Wählin, P.: GISS-E2.1: Configurations and climatology, Geoscientific Model Development, 13, 3595–3623, https://doi.org/10.5194/gmd-13-3595-2020, 2020.

Krasting, J. P., Winton, M., John, J. G., Dunne, J. P., Keyser, D., Dixon, K. W., Gnanadesikan, A., Held, I. M., Lin, S.-J., Menzel, R., Rosati, A., Seman, C. J., Underwood, S. J., and Vender, R. V. D.: The GFDL Earth System Model Version 4 (GFDL-ESM4): Model Description and Characteristics, Journal of Advances in Modeling Earth Systems, 12, e2019MS001 917, https://doi.org/10.5065/D6H70CS0, 2020.

Lee, W.-L., Yu, J.-Y., Chen, J.-P., Jiao, Y.-C., Lan, Y.-Y., Li, C.-H., Lin, P.-H., S.-Y., S. H., and Tu, C.-C.: Taiwan Earth System Model Version 1: description and evaluation of mean state, Journal of Advances in Modeling Earth Systems, 12, e2020MS002 220, https://doi.org/10.1029/2020MS002220, 2020.

Li, L., Lin, P., Yu, Y., Wang, S., Liu, Y., Xu, Y., Liu, H., Zhang, J., Ma, J., Chen, X., Sun, H., Yan, D., Wang, W., Wang, Z., Jiang, L., Yang, J., Chen, H., and Wang, H.: The CAS FGOALS-g3 model and its historical simulations for CMIP6, Journal of Advances in Modeling Earth Systems, 11, 4764–4776, https://doi.org/10.1029/2019MS001719, 2019.

Lizundia-Loiola, J., Otón, G., Ramo, R., and Chuvieco, E.: A spatio-temporal active-fire clustering approach for global burned area mapping at 250 m from MODIS data, Remote Sensing of Environment, 236, 111 493, https://doi.org/10.1016/j.rse.2019.111493, 2020.

López, L., Fisher, M., Friesz, A., Wu, Q., Steiker, A., and earthaccess community: Earthaccess: Accelerating NASA Earthdata Access Through Open, Collaborative Development, https://openscapes.org/blog/2024-03-04-earthaccess-tech-spotlight/, 2024.

Lovato, T., Peano, D., Iovino, D., Sannino, G., Cionni, I., Scoccimarro, E., Fogli, P. G., and Gualdi, S.: CMCC-ESM2: a new version of the CMCC Earth System Model for CMIP6, Geoscientific Model Development, 14, 1915–1936, https://doi.org/10.5194/gmd-14-1915-2021, 2021.

Mackallah, C., O'Neill, C., Dix, M., Bi, D., Fiedler, S., Watterson, I., Lierop, P. v., Franklin, C., Kiss, A., Hirst, A., and O'Farrell, S.: ACCESS-ESM1.5: A new generation of the Australian Community Climate and Earth System Simulator, Geoscientific Model Development, 12, 4217–4241, https://doi.org/10.5194/gmd-12-4217-2019, 2019.

Martínez, J., Vega-Garcia, C., and Chuvieco, E.: Human-caused wildfire risk rating for prevention planning in Spain, Journal of Environmental Management, 90, 1241–1252, https://doi.org/10.1016/j.jenvman.2008.07.005, 2009.

Moriondo, M. et al.: Potential impact of climate change on fire risk in the Mediterranean area, Climate Research, 31, 85–95, https://doi.org/10.3354/cr031085, 2006.

Neves, D. J. D., Silva, V. d. P. R., Almeida, R. S. R., de Sousa, F. d. A. S., and da Silva, B. B.: General aspects of the climate in the Cabo Verde archipelago, Ambiência (Online), 13, 346–355, 2017.

pandas development team, T.: pandas-dev/pandas: Pandas, https://doi.org/10.5281/zenodo.15831829, 2020.

https://doi.org/10.5194/egusphere-2026-5296
Preprint. Discussion started: 16 November 2026
© Author(s) 2026. CC BY 4.0 License.

Rew, R., Fisher, W., Davis, G., Emmerson, S., Cormack, C., Caron, J., Pincus, R., Hartnett, E., Heimbigner, D., and Appel, L.: NetCDF [Computer software], https://doi.org/10.5065/D6H70CW6, 1989.

Rodríguez Camino, E. et al.: Extreme fire weather conditions in Spain and Portugal now common due to climate change, Tech. rep., World Weather Attribution, https://doi.org/10.5281/zenodo.13682976, 2025.

Rodríguez-Rull, J., Expósito, F. J., Díaz, J. P., Carrillo, J., Pérez, J. C., and Henriques, D.: High-resolution regional climate projections and tourism impacts in the Macaronesian archipelagos, Scientific Reports, 16, 8696, https://doi.org/10.1038/s41598-026-43092-9, 2026.

Santos, F. D., Valente, M. A., Azevedo, E. B., Tomé, A. R., and Coelho, F.: Climate change scenarios in the Azores and Madeira islands, World Resource Review, 16, 473–491, 2004.

Selend, O., Lodemel, V., Tjiputra, J. F., Bentsen, M., Tveito, I. V., and Furevik, T.: NorESM2-MM: A Middle Resolution Norwegian Earth System Model for CMIP6, Geoscientific Model Development, 12, 4875–4895, https://doi.org/10.22033/ESGF/CMIP6.12608, 2019.

Semmler, T., Koldunov, N., Vancoppenolle, M., Aksenov, Y., Danilov, S., Gierz, P., Goessling, H., Madec, G., Sidorenko, D., Stanko, T., and Uotila, P.: Simulations for CMIP6 with the AWI climate model AWI-CM-1-1, Geoscientific Model Development, 13, 1003–1021, https://doi.org/10.5194/gmd-13-1003-2020, 2020.

Skamarock, W. C. et al.: A Description of the Advanced Research WRF Version 3, National Center for Atmospheric Research, Boulder, CO, USA, nCAR/TN-475+STR, 2008.

Smith, A. J. P. et al.: Climate change increases the risk of wildfires, ScienceBrief, https://doi.org/10.5281/ZENODO.4570195, 2020.

Swart, N. C., Cole, J. N. S., Kharin, V. V., Lazare, M., Scinocca, J. F., Gillett, N. P., Anstey, J., Arora, V. K., Christian, J. R., Seiler, C., and Varma, V.: The Canadian Earth System Model version 5 (CanESM5.0.3), Geoscientific Model Development, 12, 4823–4873, https://doi.org/10.5194/gmd-12-4823-2019, 2019.

Tatebe, H., Ogura, T., Nitta, T., Komuro, Y., Ogochi, K., Watanabe, S., Sekiguchi, M., Emori, S., Suzuki, T., Tateishi, T., Nishizawa, S., Suzuki, K., Shiogama, H., Mori, S., Hoshi, Y., Chikira, M., Murata, A., Jin, Z., Nozawa, T., Ohgaito, R., and Hori, M.: The Earth System Model MIROC6, Model Data Journal, 4, 22 033, https://doi.org/10.22033/ESGF/CMIP6.11322, 2019.

Turco, M. et al.: Exacerbated fires in Mediterranean Europe due to anthropogenic warming projected with non-stationary climate-fire models, Nature Communications, 9, 3821, 2018.

Van Wagner, C. E.: Development and structure of the Canadian Forest Fire Weather Index System, Tech. Rep. Forestry Technical Report 35, Canadian Forestry Service, Ottawa, ON, 1987.

Virtanen, P., Gommers, R., Oliphant, T. E., Haberland, M., Reddy, T., Cournapeau, D., Burovski, E., Peterson, P., Weckesser, W., Bright, J., van der Walt, S. J., Brett, M., Wilson, J., Millman, K. J., Mayorov, N., Nelson, A. R. J., Jones, E., Kern, R., Larson, E., Carey, C. J., Polat, İ., Feng, Y., Moore, E. W., VanderPlas, J., Laxalde, D., Perktold, J., Cimrman, R., Henriksen, I., Quintero, E. A., Harris, C. R., Archibald, A. M., Ribeiro, A. H., Pedregosa, F., van Mulbregt, P., and SciPy 1.0 Contributors: SciPy 1.0: Fundamental Algorithms for Scientific Computing in Python, Nature Methods, 17, 261–272, https://doi.org/10.1038/s41592-019-0686-2, 2020.

Volodin, E. M., Diansky, N. A., and Gusev, A. V.: INM-CM4-8 and INM-CM5.0 models and their climate sensitivity, Izvestiya, Atmospheric and Oceanic Physics, 54, 739–752, https://doi.org/10.1007/s00382-018-4422-9, 2018.

WCRP: Coupled Model Intercomparison Project, Tech. rep., World Climate Research Programme, https://wcrp-cmip.org, 2025.

Wu, T., Lu, Y., Fang, Y., Wang, Z., Lu, Y., Li, Q., Liu, P., Zhang, J., Song, M., Zhu, X., Zhang, H., Chen, Q., Chen, Z., Wu, L., Li, C., Jia, Z., Ma, H., Zhang, Y., Yu, Y., Liu, J., Xie, Y., Ma, J., and Wu, Y.: The Beijing Climate Center Earth System Model version 2 (BCC-ESM2), Journal of Advances in Modeling Earth Systems, 11, 4742–4763, https://doi.org/10.1029/2019MS001768, 2019.

https://doi.org/10.5194/egusphere-2026-5296
Preprint. Discussion started: 16 November 2026
© Author(s) 2026. CC BY 4.0 License.



Yukimoto, S., Adachi, Y., Hosaka, M., Bunya, S., Deushi, M., Hirai, M., Mizuta, R., Ose, T., Sachweh, B. A., Tanaka, T., TATEBE, H., and Tokioka, T.: The Meteorological Research Institute Earth System Model Version 2.0 (MRI-ESM2.0): Description and Basic Evaluation of the Decadal Prediction Experiments, Journal of Climate, 33, 1–25, https://doi.org/10.1175/JCLI-D-19-0298.1, 2020.